ICARUS 91, 220–233 (1991)

# Possible Microwave Absorption by $H_2S$ Gas in Uranus' and Neptune's Atmospheres

IMKE DE PATER

*Astronomy Department, 601 Campbell Hall, University of California, Berkeley, California 94720*

PAUL N. ROMANI

*Science Systems and Applications, Inc., 7275 Executive Place, Suite 300, Seabrook, Maryland 20706*

AND

SUSHIL K. ATREYA

*Department of Atmospheric, Oceanic, and Space Sciences, University of Michigan, Ann Arbor, Michigan 48109*

Received May 25, 1990; revised February 12, 1991

**We present new VLA observations of Neptune at 3.55 and 20.1 cm. The disk-averaged brightness temperatures are 191.2 ± 6 K at 3.55 cm, and 276.4 ± 10 K at 20.1 cm. These values are consistent with thermal spectra of the planet. We further present a comparison between Uranus and Neptune's spectrum, using improved atmospheric models for both planets. We improved the old models by including microwave absorption by $H_2S$. The rotational lines of this gas, which are all at (sub)millimeter wavelengths, are pressure broadened to such an extent that considerable opacity at centimeter wavelengths is expected. We estimate from our calculations that the $H_2S$ mixing ratio on Uranus and Neptune is likely enhanced by a factor of 10–30 above the solar sulfur elemental ratio, and that the S/N ratio must exceed 5 × the solar ratio. Our calculations suggest the width of the $H_2S$ line to be similar to or less than that of water. There is more microwave opacity in Neptune's atmosphere than in that of Uranus, which may be caused by the presence of some $NH_3$ gas above the $NH_4SH$ cloud layer. From a comparison with the radio occultation data, we suggest that $NH_3$ is likely supersaturated in Neptune's atmosphere at levels where $T \lesssim 210$–225 K, or $P \lesssim 20$–25 bar.** 

## 1. INTRODUCTION

Previous work regarding microwave spectra of Uranus and Neptune suggested that the spectra of these planets were rather different (de Pater *et al.* 1989, Romani *et al.* 1989, hereafter called PRA and RPA, respectively): Uranus' spectrum rises steeply from ~1 to 6 cm, and is nearly constant at ~260 K at longer wavelengths; Neptune's spectrum seems to rise continuously up to ~320 K at 20 cm. The latter brightness temperature seemed to be ~60 K higher than predicted from model calculations for an atmosphere with a composition similar to that of Uranus (RPA), and suggested an excess of emission at this wavelength. It was suggested (de Pater and Richmond 1989, de Pater and Goertz 1989) that this excess emission could be due to nonthermal or synchrotron radiation from relativistic electrons in a Neptunian magnetic field. However, the Voyager 2 spacecraft failed to detect energetic electrons (Stone *et al.* 1989). This implies that all the microwave emission from Neptune must be of thermal origin.

RPA showed attempts to fit Neptune's radio spectrum under the assumption that the observed spectrum was entirely of thermal origin. They could only obtain fits to the spectrum if $NH_3$ gas was depleted by a factor of ~50 compared to the solar N value throughout the region of the atmosphere probed at centimeter wavelengths. Since the Voyager spacecraft did not detect any $N_2$ signature at Neptune, the low $NH_3$ abundance suggested a large global nitrogen depletion on Neptune. Such a depletion is inconsistent with current theories regarding the formation of the giant planets. Even if there was a lack of nitrogen-bearing solids in the primitive solar nebula during the accretion phase of the outer planets (e.g., most N is in the form of $N_2$), one would expect a solar N/H ratio in the planet's deep atmospheres below the level of any cloud formation. In addition, one would expect Uranus and Neptune to be similar in composition since the physical conditions in the primitive solar nebula are expected to be very much alike in the regions where these two planets formed. PRA showed that Uranus' radio spectrum is consistent with a bulk ammonia abundance equal to the solar value or larger in its deep atmosphere ($P \gtrsim 50$ bar). The gas will be depleted at higher levels in the atmosphere due



0019-1035/91 $3.00

to cloud formation (the solution cloud as well as the $NH_4SH$ cloud).

To investigate the discrepancy between the microwave spectra of Uranus and Neptune in more detail, we observed Neptune again at a 20-cm wavelength, with better accuracy. These data are reported in this paper, together with observations at 3.55 cm.

In addition, we carefully reexamined the model atmosphere calculations of both Uranus and Neptune. In particular, we investigated the effect on the planet's microwave spectra due to absorption by $H_2S$ gas.

## 2. OBSERVATIONS, DATA REDUCTION, AND RESULTS

### *2a. Observations*

We observed Neptune with the VLA (Very Large Array) of the National Radio Astronomy Observatory[1], on April 15, 16 and 19, 1990, at wavelengths of 20.1 and 3.55 cm. We observed simultaneously at frequencies 1465 and 1515 MHz, and 8415 and 8465 MHz, each with a 50-MHz bandwidth. The VLA was in its most extended, or A-configuration. The total integration time at 20.1 cm was about 15 hr, and at 3.55 cm about 3 hr. Our prime interest was to obtain a good measurement at 20 cm; we, therefore, spent all the night time observing at 20 cm (when the ionosphere is quietest), and scheduled 1.5 hr at the end of each run at 3.55 cm. Since the latter data are all at the same hour angle, the image of the planet at 3.55 cm is not as good as we would have liked. At the time of our observations, Neptune's diameter was 2.25″.

The data were calibrated against 3C286, for which we assumed flux densities of: 14.635 Jy at 1465 MHz, 14.399 Jy at 1515 MHz, 5.280 Jy at 8415 MHz, and 5.259 Jy at 8465 MHz (Baars *et al.* 1977). Since Klein (1985 private communication; see also de Pater and Gulkis 1988) suggested the flux density of 3C286 to be too low at 3.55 cm by ~3%, we increased the flux density of Neptune at this wavelength by 3%. We believe the internal calibration to be accurate to within 2% (e.g., de Pater and Gulkis 1988); and added the latter uncertainty to the error estimates in the measured flux densities. In addition, the final flux densities reported in the paper were increased by 2.7 K to correct for the microwave background. This was not done for VLA data on Uranus and Neptune reported earlier (de Pater and Gulkis 1988, de Pater and Richmond 1989); we included this effect for the spectra displayed in this paper. The complex gain of each antenna was monitored every 25 min by observations of 1911-201, which appeared to have a flux density of ~2.2 Jy at both 3.55 and 20.1 cm.

[1] The VLA is operated by the National Radio Astronomy Observatory, which is operated by the Associated Universities, Inc., under contract with the National Science Foundation.

### *2b. Flux Density Measurements*

As shown by de Pater and Gulkis (1988), the visibility or UV data at short baselines can be used to measure the total flux density from Neptune. Figure 1 shows the real part of the visibility data at 20.1 and 3.55 cm, together with the Bessel function (solid line) which gave the best fit to the zero-spacing flux density. Only data at $\beta < 0.4$ were included in the fit ($\beta = rB$, with $r$ = radius of the planet in radians, and $B$ = projected baseline in units of wavelengths), as suggested by de Pater and Gulkis (1988). Since we used the real part of the data rather than the amplitude visibility, we fitted the data with a disk offset from the center; the offset was measured from images at the two wavelengths (~0.4″ at each wavelength). The result at 20 cm is 1.75 ± 0.05 mJy, which translates into a disk-averaged brightness temperature of 273.7 ± 8 K. At 3.55 cm we determined a flux density of 37.5 ± 1 mJy, or 183.0 ± 5 K. After correction for the flux density of 3C286 (3% at 3.55 cm), the microwave background (2.7 K), and inclusion of the internal calibration uncertainty, we get the following radio brightness temperatures for Neptune: 276.4 ± 10 K at 20.1 cm, and 191.2 ± 6 K at 3.55 cm.

### *2c. Images*

We Fourier transformed the visibility data to obtain images of the planet at both wavelengths. We used the standard NRAO–AIPS reduction package. We choose the natural weight option (e.g., Sramek and Schwab 1989, de Pater 1990) which is best for weak sources. The planet was more or less unresolved at 20 cm, so we used the conventional CLEANing technique (Högbom 1974, Clark 1980) to remove the instrumental response from the image. At 3.55 cm, the planet is resolved, and we used the planetary CLEANing technique. These data were also self-calibrated to reduce phase errors in the image (e.g., de Pater 1990). The results are shown in Fig. 2. The resolution at 20 cm was too low to resolve the planet; at 3.55 cm there are about eight resolution elements across the disk (beam size 0.26″). The disk appears to be rather symmetric. Unfortunately, the quality of the 3-cm image is too low to allow detailed interpretation of limb darkening curves. In addition to the images displayed in Fig. 2, we also made maps at 20 cm for each day and frequency (1465 and 1515 MHz) separately. We obtained three different maps for each dataset, using taper functions of 60, 100, and 150 kilowavelengths (Gaussian taper applied to the UV data, such that the weight is 30% at 60, 100, and 150 kilowavelengths, respectively). We determined the total

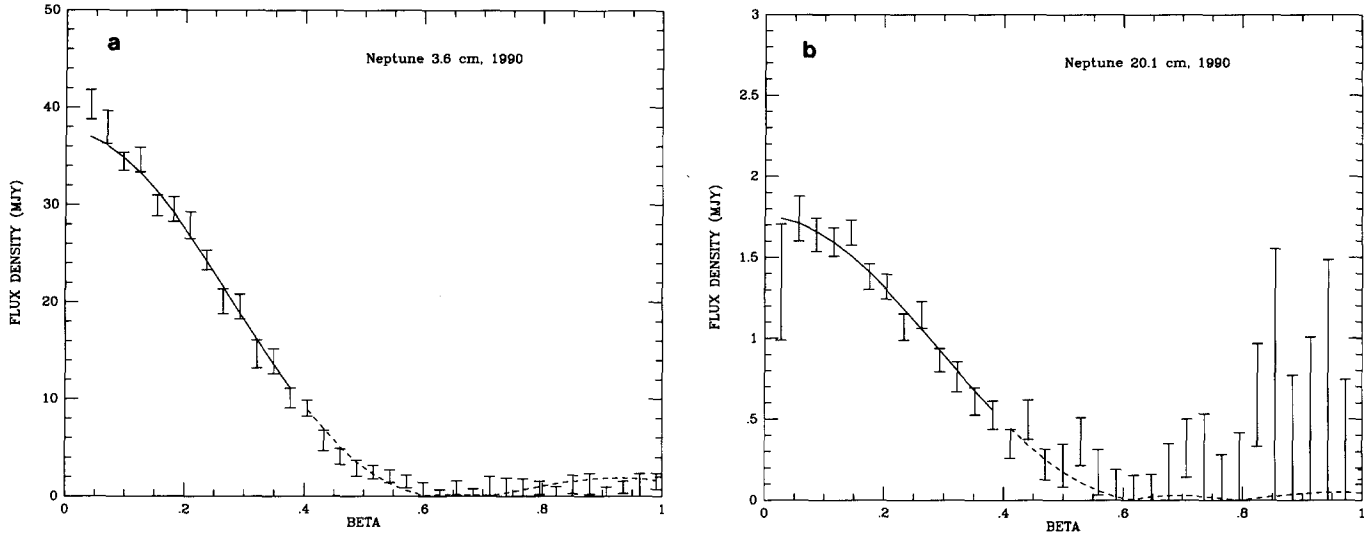


FIG. 1. The real part of the visibility data of Neptune at 3.55 cm (a) and 20.1 cm (b). Superimposed is the best fit Bessel function to determine the zero-spacing flux density.

flux densities from these maps, which varied from 1.60 to 1.90 mJy, with an average of 1.71 ± 0.12 mJy. The total flux density from all data combined (Fig. 2) is 1.66 ± 0.04 mJy, ~5% below the zero-spacing flux density as determined from the visibilities. As pointed out by de Pater and Gulkis (1988), it is quite common to find map values ~5% below the values determined from the visibility data, for example due to small phase errors in the data.

## 3. DISCUSSION

### *3a. Atmospheric Model*

Radio spectra of the planets are usually analyzed by comparing the observed spectra with synthetic spectra, obtained by integrating the equation of radiative transfer

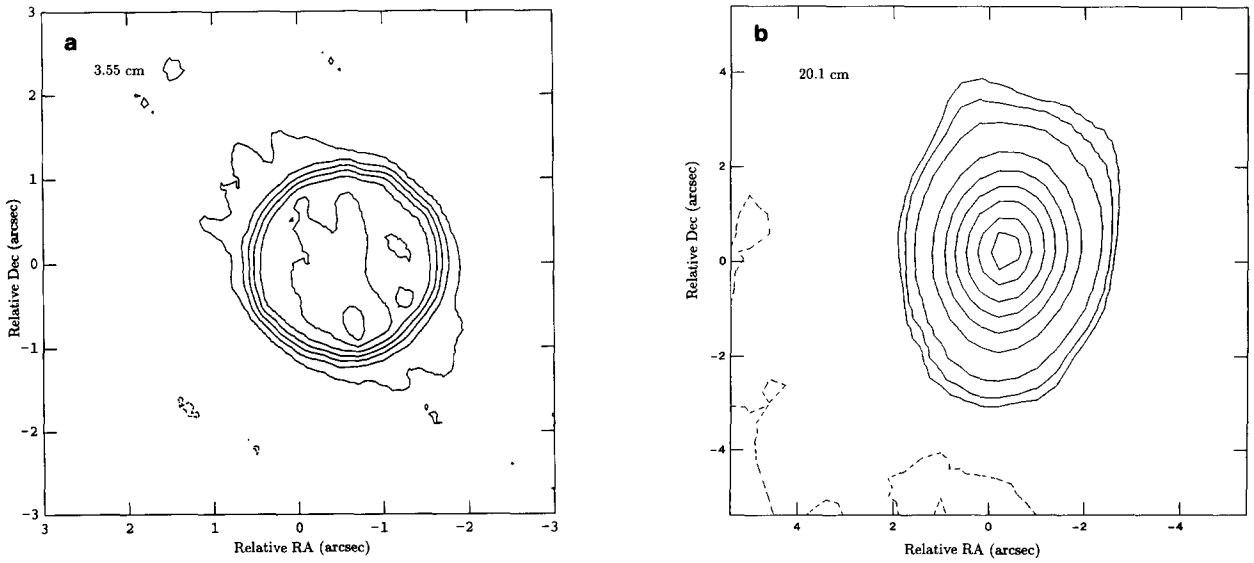


FIG. 2. Images of Neptune at 3.55 cm (a), and 20.1 cm (b). The beam size was 0.26″ (a), and 2.62 × 1.66″ (b), respectively. Contour values in Kelvin are: (a) 25, 63, 101, 140, 177, 215, 240 K; (b) 4.4, 7.4, 15, 37, 59, 81, 103, 126, 140 K. (Note that the source in b is unresolved, and thus a brightness temperature less than the disk-averaged value.

through a model atmosphere. The atmospheric model used in these calculations is a simple lifting parcel model that has been described extensively before (PRA, RPA). The calculations start deep in the atmosphere below the formation of suspected clouds (aqueous ammonia solution, ammonium hydrosulfide solid, water ice, ammonia ice, hydrogen sulfide ice, methane ice, and argon ice), with a specified composition, temperature, and pressure. The model steps up in altitude and the new temperature is calculated from the dry or appropriate wet adiabatic lapse rate and the new pressure by assuming hydrostatic equilibrium. The partial pressures of all constituents are calculated assuming the atmosphere to be an ideal gas. From the new temperature and empirical formulas the equilibrium saturation vapor pressures of all possible condensates are calculated. If the partial pressure of a condensate in the atmosphere exceeds its respective saturation vapor pressure, then a cloud forms and the atmospheric partial pressure of the condensing species is set equal to its equilibrium saturation pressure. We use the same vapor pressure equations as those used in PRA, with the exception of that of $H_2S$ over $H_2S$–ice. We are now using a curve fit to the recent data of Kraus *et al.* (1989). Their data extend from the triple point (188 K) of $H_2S$ to 113 K, and the curve fit reproduces the data to within an average error of 9%. If $H_2S$ was greater than or equal to 500 × solar, then a thin $H_2S$ liquid cloud would form and we used the vapor pressure data from Giauque and Blue (1936) for that cloud. The sinks for $H_2S$ from the vapor phase are then: the aqueous ammonia solution cloud, ammonium hydrosulfide cloud, and liquid/ice $H_2S$ cloud. For $NH_3$ the sinks are the same with the exception, of course, it condenses to its own ice cloud.

The base level composition is for 1 mol of gas for which the $He/H_2$ ratio is 0.18 by number, and the other trace gases $H_2O$, $CH_4$, $NH_3$, $H_2S$, and Ar are present in selected enrichments to solar. Our solar values are based upon Cameron (1982). Recently, Anders and Grevesse (1989) have reviewed the literature and proposed new solar values. In comparison, the Cameron values need to be multiplied by the following factors to agree with the Anders and Grevesse numbers: 0.87 for $C/H_2$, 1.3 for $N/H_2$, and 1.2 for $O/H_2$. The relative $He/H_2$ ratio in our model is in conformity with our previous Uranus studies and is based on the Voyager 2 IRIS determination for Uranus (Conrath *et al.* 1987). It is also within error bounds of the solar $He/H_2$ ratio, and the value adopted for Neptune (Lindal *et al.* 1990). For all studies $CH_4$ was held at 30× solar to reproduce approximately the observed 2% mixing ratio in the upper troposphere before the $CH_4$–ice cloud begins to form. (Lindal *et al.* 1987, Orton *et al.* 1987). Studies in the IR indicate that Neptune and Uranus have similar temperatures at the 1-bar level (Orton *et al.* 1987), so we have chosen the temperature and pressure of the base level to reproduce the observed 101 K at 2.3 bars on Uranus by the Voyager RSS (Lindal *et al.* 1987). For Neptune, this translates into a temperature of about 79 K at 1.2 bars, close to the value (78 K) reported by Tyler *et al.* (1989) from the radio occultation experiment aboard Voyager 2.

To date models of the radio spectra of Uranus and Neptune included the following microwave absorbers: $NH_3$–gas, $H_2O$ vapor and droplets, and collision-induced absorption by $H_2$ ($H_2$–$H_2$, $H_2$–He, $H_2$–$CH_4$) (e.g., Berge and Gulkis 1976, de Pater and Massie 1985). Several other gases, such as $PH_3$, $H_2S$, CO, HCN, are known to absorb at submillimeter and millimeter wavelengths. $PH_3$, CO, and HCN have been seen in the IR on Jupiter and Saturn, but have never been detected at microwave wavelengths, since their abundances are too small to noticeably affect the microwave spectra (see, e.g., Lellouch *et al.* 1984 for synthetic spectra of Jupiter and Saturn). $H_2S$ has never been detected at IR or radio wavelengths. Hence, microwave absorption by any of these gases is usually ignored in atmospheric modeling studies.

In our previous papers (PRA; RPA) we suggested mixing ratios for $H_2S$ gas exceeding 100 × solar S. The rotational lines of $H_2S$ are all at submillimeter and millimeter wavelengths, where one probes temperatures $\lesssim$100 K. At these low temperatures $H_2S$ gas will be completely condensed out ($NH_4SH$–solid, $H_2S$–ice/liquid), and hence no absorption is expected. However, with the large $H_2S$ mixing ratios in Uranus and Neptune's atmospheres, and the high pressures probed at radio wavelengths (which will broaden the lines considerably), absorption at centimeter wavelengths can be significant. We, therefore, improved our model by including microwave absorption by $H_2S$ gas in our calculations. We included the rotational lines at the following frequencies: 168.762, 216.710, 300.505, 369.101, and 369.126 GHz. The line intensities were taken from the Poynter and Pickett catalogue (Poynter and Pickett 1981), and are very similar to the values given in the GEISA data bank (Flaud *et al.* 1983). The line width due to collisional broadening in a hydrogen–helium–methane gas mixture is not known. We assumed it to be similar to the line width of water (as given by Berge and Gulkis 1976), and used a value of 2.4 GHz at 1 bar and 273 K, with a temperature dependence $(273/T)^{2/3}$. The lineshape was approximated by a Van Vleck–Weisskopf line profile. As a check on our model, we calculated Jupiter's spectrum with an $H_2S$ abundance similar to that used by Bezard *et al.* (1983). Our results agree well with their model spectra.

### *3b. Uranus*

*3b1. Spectrum.* Interpretation of Uranus' spectrum by model fitting the data is severely limited by the large

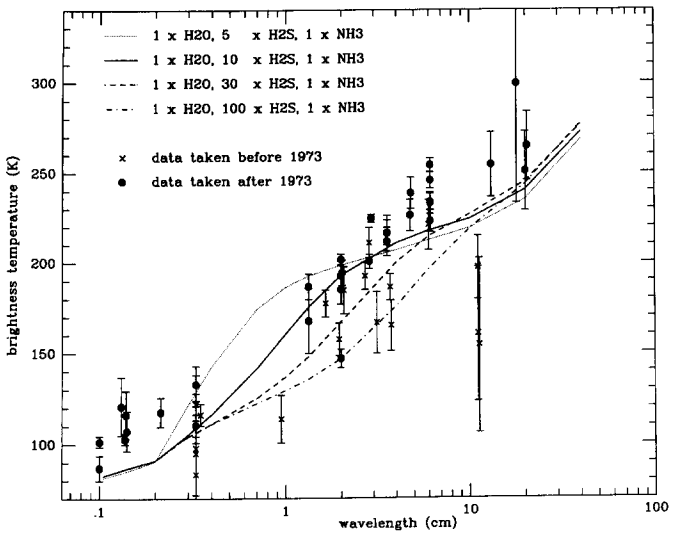


FIG. 3. Uranus' spectrum with superimposed model atmosphere calculations to show the effect of a change in the $H_2S$ mixing ratio on the microwave spectrum.

spread in brightness temperatures at individual wavelengths. For example, at 6 cm we see six data points with temperatures between 220 and 255 K, none of them particularly better than others. Also at other wavelengths large differences in brightness temperature exist, between data points with relatively small error bars. The cause of this spread is unknown, and could be due to time variability. In this paper we will limit ourselves to obtaining fits which more or less mimic the shape of the spectrum as indicated by the filled circles. We ignore the data indicated by crosses, which were taken before 1973, when Uranus gradually "warmed" due to the changing viewing aspect of the planet (e.g., Gulkis *et al.* 1983).

Results of model atmosphere calculations for Uranus are displayed in Figs. 3–6. Figure 3 shows model spectra for an atmosphere with solar abundances of $H_2O$ and $NH_3$, and $H_2S$ equal to 5×, 10×, 30×, and 100× the solar S value. As noted before (PRA), the long wavelength part of the spectrum (≳4 cm) can only be matched if $NH_3$ gas is depleted deep in the atmosphere. The depletion is likely due to the formation of an $NH_4SH$ cloud (Gulkis *et al.* 1978, Lewis and Prinn 1980). Since the altitude of this cloud depends upon the abundance of both $H_2S$ and $NH_3$ gases, PRA inferred from a comparison between the data and models that the $H_2S$ mixing ratio has to exceed 10–30× solar S to match the data longward of ~4 cm. In addition, the S/N ratio has to exceed 5× the solar ratio.

We like to stress here the difference between our old and new calculations: With our old thermochemical equilibrium calculations we could fit Uranus' spectrum longward of ~4 cm reasonably well, if the $H_2S$ mixing ratio did exceed 10–30× the solar S value. However, in doing so the synthetic spectrum was always too warm at shorter wavelengths, which implied the presence of an extra source of opacity at these wavelengths, or altitudes, in the atmosphere. A good fit could be obtained by assuming a constant value of $\sim 5 \times 10^{-7}$ for the ammonia mixing ratio between the $NH_3$–ice cloud and levels near 240 K (~30 bar). The $NH_3$ mixing ratio had to exceed the solar N value at deeper levels in the atmosphere ($T \gtrsim 270$ K, or $P \gtrsim 50$ bar) to fit the data longward of ~10 cm. Such an $NH_3$ mixing ratio profile could be obtained either by assuming a rapid vertical mixing process, or by assuming $NH_3$ gas to be supersaturated above the $NH_4SH$ cloud, at altitudes, where $T < 240$–245 K. Both processes result in an effective increase in the ammonia mixing ratio, and thus opacity, at higher levels in the atmosphere. In the new calculations, the extra opacity at short centimeter wavelengths is provided by microwave absorption from $H_2S$–gas.

To better show the differences and similarities between the various models, Fig. 4 shows weighting functions in Uranus' atmosphere at 2, 6, and 20 cm. We assumed solar abundances for water and ammonia gas, and an enhancement in $H_2S$ gas by a factor of 10 above solar S. Figure 4a shows the old equilibrium model, without microwave abosrption by $H_2S$ gas; Fig. 4b shows the old supersaturation model (no $H_2S$ absorption), and Fig. 4c shows the weighting functions for the new equilibrium calculations, which include $H_2S$ absorption. In addition, the temperature–pressure profile, and mixing ratios of $NH_3$, $H_2S$, and $H_2O$ gas are shown.

At wavelengths longward of ~4 cm, the results from the old models in chemical equilibrium (no supersaturation or mixing) and the new models (inclusion $H_2S$ absorption) are similar if the enhancement in the $H_2S$ mixing ratio is ≲20× solar S: the brightness temperature of the planet increases with increasing $H_2S$ mixing ratio, since the formation of the $NH_4SH$ layer, and therefore depletion in $NH_3$ gas, is pushed to deeper levels in the atmosphere. For calculations with enhancements above ~20× solar S the microwave opacity at these long wavelengths will be increased, and the brightness temperature of the planet will decrease.

As mentioned above, the line width of $H_2S$ in a $H_2$–He gas mixture at these (or other) pressures has never been measured. We, therefore, also investigated the effect on the microwave spectra by varying the line width. The line width of water due to foreign gas broadening has been measured at different frequencies for various gas mixtures. Variations by a factor of ~2 are common. Figure 5 shows the changes on Uranus' synthetic spectrum for a line which is 3× broader and 3× smaller than that of water. In these calculations we assumed an atmosphere in which $H_2S$ is enhanced 20× above solar S, while $H_2O$ and $NH_3$ are present in solar abundances. Thus, if the

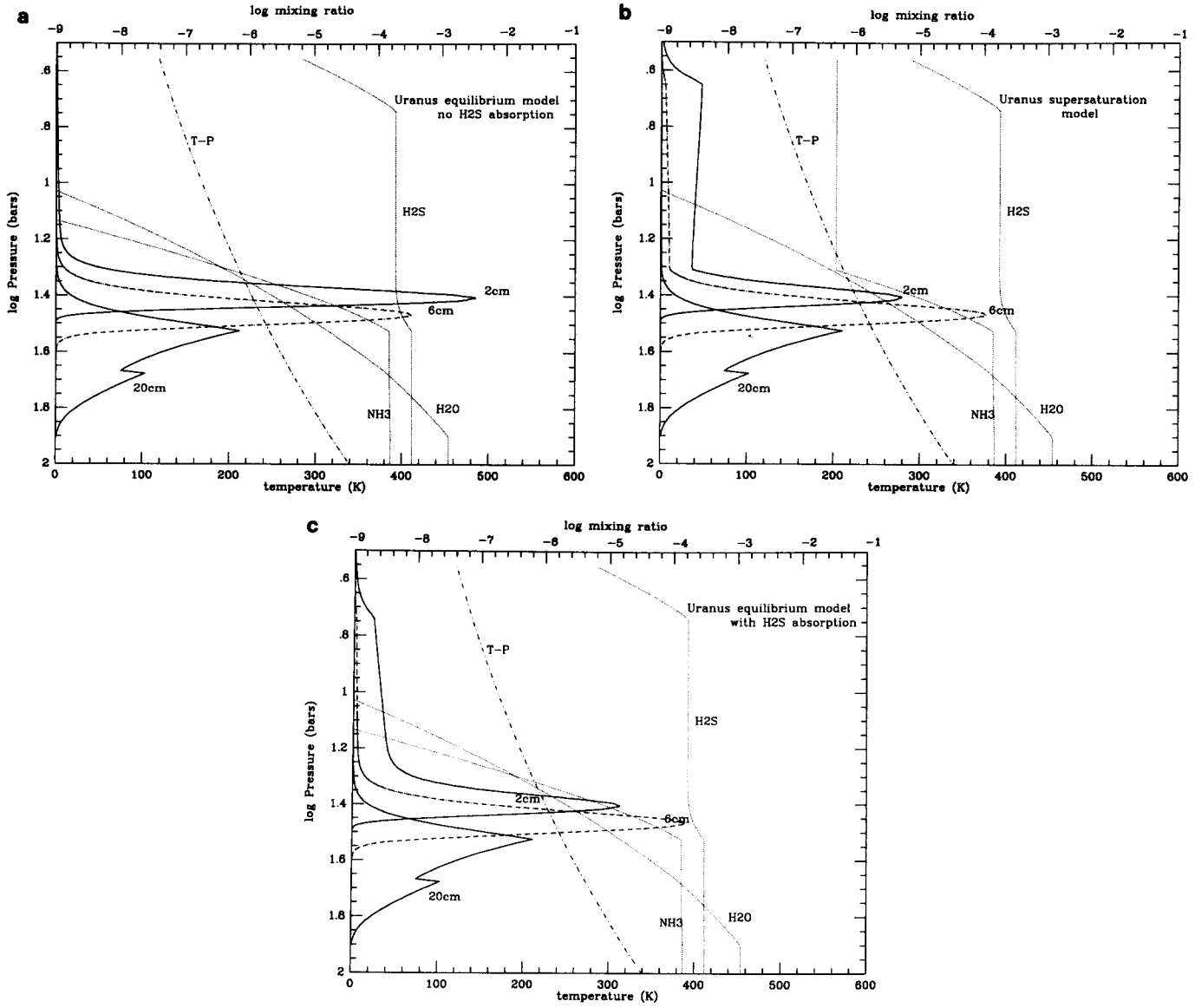


FIG. 4. Weighting functions in the Uranian atmosphere at 2, 6, and 20 cm. The functions are for an atmosphere with solar abundances for $H_2O$ and $NH_3$, and an enhancement in $H_2S$ by a factor of 10 above solar S. The abundances of the various elements are shown by the dotted curves, and the temperature–pressure profile in the atmosphere by the dot–dash line. (a) Old equlibrium model without microwave absorption by $H_2S$ gas; (b) old supersaturation model, where $NH_3$ is supersaturated in the atmosphere at $T \lesssim 210$ K ($P \lesssim 20$ bar) with a mixing ratio of $5 \times 10^{-7}$; (c) new equilibrium calculations, which include microwave absorption by $H_2S$ gas.

$H_2S$ line width is narrower than that of water, the $H_2S$ abundance in Uranus' atmosphere needs to be increased to match the observed spectra; if it is broader it should be decreased. However, even in the latter case, the enhancement in $H_2S$ must exceed $\sim 10\times$ solar S to remove the $NH_3$ deep enough in the atmosphere, so the long wavelength range of Uranus' spectrum can be matched. This suggests that the width of the $H_2S$ line is similar to or smaller than the width of the water line. If the $H_2S$ mixing ratio would be equal to $20\times$ solar S, the $H_2S$ line width should be ~one-third that of water to match Uranus' spectrum (Fig. 5), and if the $H_2S$ abundance is equal to $60\times$ solar S the line width would have to be ~one-fifth that of water.

We note that the models which mimic the short wavelength range of Uranus' spectrum do not match the data longward of 4–6 cm very well, although they are consistent with the data to within the uncertainties. An increase in the $H_2S$ abundance to 60 or $100\times$ solar S, with a simultaneous decrease in the line width does match the spec-

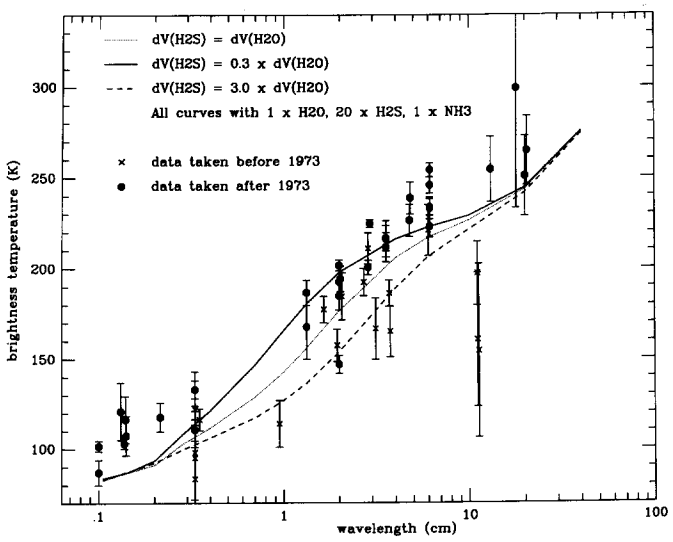


FIG. 5. Uranus spectrum with superimposed model atmosphere calculations in which the $H_2S$ line width was taken to be 3× larger and smaller than that of water, respectively. We used a solar composition atmosphere for the two planets, with $H_2S$ 20× enriched above the solar S value.

trum rather well. However, based upon the similarities between $H_2O$ and $H_2S$ molecules, we do not believe that the line width is much less than half the width of the water line.

Changes in the spectrum by an increase in the water abundance to enhancements similar to that of $H_2S$ are very small. We, therefore, do not show such spectra here. Changes in the $NH_3$ mixing ratio will modify the shape of the spectrum somewhat. Figure 6 shows calculations for an $H_2S$ abundance equal to 10 and 30× solar S, and an ammonia abundance of 0.01, 1.0, and 5× the solar N value. The three models are rather similar shortward of ~10 cm, and, as expected, the model with the low ammonia mixing ratio results in the highest brightness temperature at 20 cm. The brightness temperature near 6 cm wavelength can only be increased if, in addition to a low ammonia abundance, the opacity in the solution cloud is less than what is in the model. The dot–dash curve on Fig. 6 shows the result when we decrease the cloud opacity by a factor of 3.

The computed cloud densities in the model are the same as adiabatic liquid water contents for terrestrial clouds, i.e., maximum cloud densities based upon the assumption of no loss by precipitation. When terrestrial cloud densities are compared to the adiabatic cloud content they are between 0.2 and 0.6 of the adiabatic cloud value (see Fig. 2–15 in Pruppacher and Klett 1980). So it is not unreasonable that on Uranus the solution cloud density is lower than the model predicted. Since the solution cloud is an important source of opacity at 6 cm, variability in the cloud density could naturally explain the large spread in the 6-cm brightness temperatures.

We also considered to truncating the $H_2S$ line shape at some distance from the line center. Such a method was used by Bezard *et al.* (1983) to better match the true absorption profile in the far wings of the Lorentzian line shape they used. The resulting microwave profile was changed noticable only when the line was truncated close to the line center, ~10–20 half-widths. In addition to the fact that this is unrealistic, the effect was much more pronounced at short centimeter wavelengths than at the longer wavelengths.

*3b2. Spatial brightness distribution.* PRA assigned typical brightness temperatures on Uranus to the polar region (S. latitudes $\phi > 70°$), midlatitudes ($30–40° < \phi < 70°$), and equator ($\phi < 30–40°$; note PRA's statement that due to the viewing geometry, the temperature at $\phi < 10°$ cannot be determined) at 6 and 2 cm: near the pole: 270–280 K (6 cm) and 240–250 K (2 cm); at midlatitudes: 250 K (6 cm) and 200–220 K (2 cm); near the equator: 220 K (6 cm) and 160–170 K (2 cm). Since the pole-to-equator temperature gradient is much larger than that expected from limb darkening calculations alone (e.g., Gulkis and de Pater 1984, PRA), this temperature gradient implies a change in opacity between the pole and equator (a pole-to-equator gradient in the physical temperature appeared unrealistic; e.g., Gulkis and de Pater 1984). PRA suggested the ammonia mixing ratio to be largest in the equatorial region ($2 \times 10^{-6}$), and smallest near the pole ($\sim 10^{-7}$). The $NH_3$ mixing ratio was greater than solar

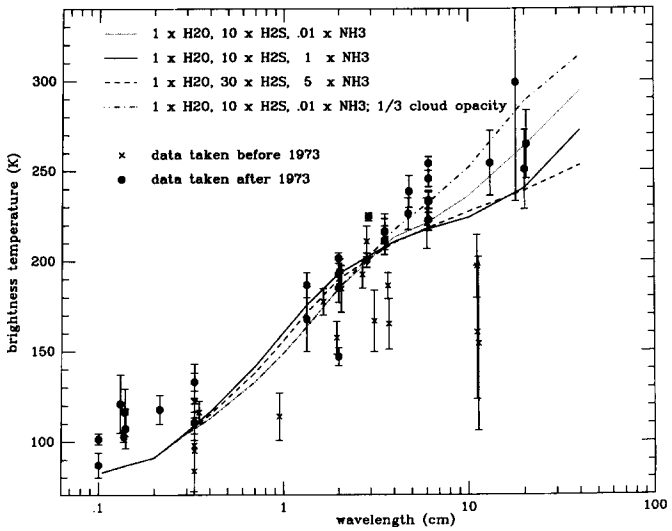


FIG. 6. Uranus spectrum with model atmosphere calculations which show the effect of changing the $NH_3$ abundance in the atmosphere, from 0.1 to 5× solar N. The calculations are for a solar $H_2O$ mixing ratio, and $H_2S$ gas enhanced by a factor of 10 and 30 above solar S, as indicated on the figure.

and homogeneous in latitude below the level of cloud formation. Since a major source of opacity in our new calculations is $H_2S$ gas in addition to ammonia gas and water vapor/droplets, we reassessed our previous conclusions.

A local depletion or enhancement of the gases in Uranus' atmosphere is most likely caused by dynamical processes in its atmosphere, such as subsidence and upwelling. We, therefore, assumed the effect to be equally effective on all gases and droplets, and assumed all of them to be depleted or enhanced by the same factor. We used solar mixing ratios for $H_2O$ and $NH_3$ in our nominal model, and 10× solar S for $H_2S$. To match the observed brightness temperature at the pole, all gases and droplets need to be depleted by a factor of ~50–100 compared to the nominal model, down to depths of ~50 bar. At midlatitudes the constituents need to be depleted by a factor of ~10, and at the equator an enhancement by a factor of ~5 is needed, down to ~20 bar or deeper. In the latter calculations we did not allow gases to be supersaturated; so in essence, only the $H_2S$ mixing ratio was enhanced by this factor, since both $H_2O$ and $NH_3$ follow the saturated vapor curves ($NH_3$ follows the vapor curve above an $NH_4SH$ cloud).

*3b3. Circulation model.* From a simple solar insolation model one would expect Uranus' pole to be warmer than the equator by ~6 K. However, Voyager IRIS measurements show that Uranus' effective temperature is remarkably similar at all latitudes. This suggests a redistribution of heat due to dynamical processes in Uranus atmosphere or interior (e.g., Conrath *et al.* 1988). A simple redistribution of heat in the upper troposphere could be due to meridional heat transport in a Hadley cell circulation, where air rises at the hot pole, and sinks back into the atmosphere at the equator. In contrast to atmospheric heat transport, it can also take place in the planet's interior. Ingersoll and Porco (1978) show that on Jupiter the internal heat flux increases with latitude, such as to maintain a nearly constant heat flux out of the planet. They show that such a redistribution would occur if the interior of the planet were convective. No rigorous models of the interior dynamics of Uranus exist to prove or disprove whether the radiogenic source alone can render the interior of Uranus convective. The work of Ingersoll and Porco (1978) and Friedson and Ingersoll (1987), however, suggests that the internal heat flux should exceed the absorbed solar flux at Uranus and Neptune by at least 27% for their interiors to be convective. The upper limit to the internal heat flux on Uranus, 14% of the absorbed solar flux (Conrath *et al.* 1988), although greater than the radiogenic heating, is far less than the above mentioned value of 27% needed for the complete redistribution of heat in the planet's interior.

The radio data discussed in this paper suggest a relative depletion of gases near the pole and at midlatitudes, with an enhancement at lower latitudes. This implies the following general circulation model for Uranus: air is rising at low latitudes ($\phi < 30$–$40°$) and subsiding at all other latitudes. Where gas is rising, it will cool off and condense out when the partial pressure falls below the saturated vapor pressure. The subsequent subsidence of this relatively dry gas at other latitudes will cause subsaturation at these latitudes, similar to the process seen between the zones and belts on Jupiter (e.g., de Pater 1986). This circulation model is just opposite to that expected from a simple Hadley cell circulation due to solar insolation. Since we probe well below the region heated by sunlight, our data suggest that at least part of Uranus' heat redistribution is controlled by the internal heat flux. However, as mentioned above, this seems to be inconsistent with *current* radiative–convective–dynamic models of the giant planet atmospheres.

Our model may be consistent with the meridional flow model proposed by Flasar *et al.* (1987) based upon the Voyager IRIS data. In their model, air rises approximately between S. latitudes of 20 and 40°, and subsides at all other latitudes. Since we cannot infer accurate brightness temperatures from the radio data at latitudes below ~10° due to the viewing geometry, our circulation model may be consistent with Flasar *et al.*'s flow model. Both models also agree with that suggested by Hofstadter *et al.* (1990), but note that they used a rather simple atmospheric model to analyze 6-cm radio data (no cloud chemistry, nor microwave absorption by $H_2S$ was included in their models). The circulation model proposed by PRA based upon their supersaturation model is slightly different, in that upwelling occurred at slightly higher S. latitudes (30–60°). However, even that model may agree with Flasar *et al.*'s meridional flow model.

### *3c. Neptune*

*3c1. Spectrum.* As described in section 2, our result for the disk-averaged brightness temperature of Neptune is 191.2 ± 6 K at 3.55 cm, and 276.4 ± 10 K at 20.1 cm. The spectrum is shown in Fig. 7, with superimposed model calculations from RPA. The dotted line is for a solar composition atmosphere. The dashed line is for a similar atmosphere, but $NH_3$ gas is depleted by a factor of ~50 throughout the atmosphere. The solid lines are calculations for an atmosphere in which both $H_2O$ and $H_2S$ are enhanced by a factor of 500 above solar O and S, respectively, and $NH_3$ by a factor of 15. In the latter calculations, ammonia gas is depleted at higher altitudes due to cloud formation (solution cloud, $NH_4SH$ cloud, and $NH_3$–ice). The upper solid line is a calculation in chemical equilibrium, the lower line is one in which we

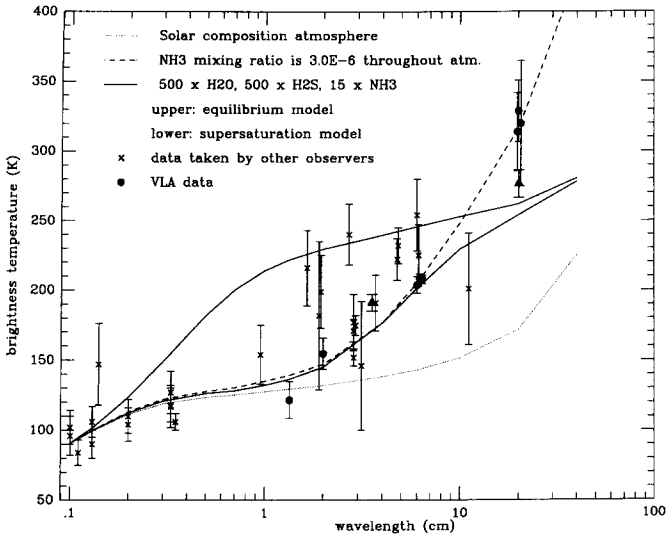


FIG. 7. Neptune's spectrum with superimposed model atmosphere calculations from RPA. The new data are indicated with triangles.

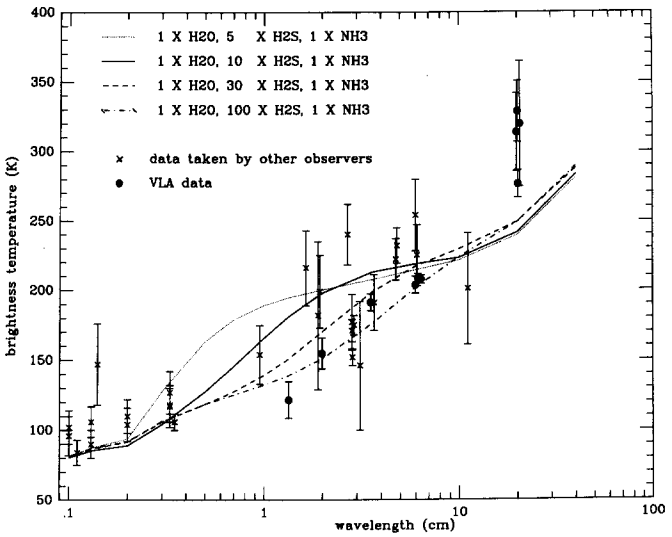


FIG. 8. Neptune's spectrum with superimposed various model atmosphere calculations to show the effect of changing the $H_2S$ abundance in the atmosphere.

assumed the atmosphere to be supersaturated in $NH_3$ at temperatures $T \lesssim 240$ K. As shown, the new data points are rather close to the last model curve (lower solid line). The new 20-cm data point is well below the central values reported by de Pater and Richmond (1989), but within the errorbounds; the data point has a better accuracy due to a longer integration time and due to less confusion by background sources. The image is much "cleaner" than the previous images, and the visibility curve is better defined.

We show various synthetic spectra from our new atmospheric calculations (chemical equilibrium, with inclusion of microwave absorption by $H_2S$ gas) in Fig. 8. In these calculations we assumed a solar composition atmosphere, and enhanced the $H_2S$ abundance above solar S by a factor of 5, 10, 30, and 100, respectively. The last model fits the data best. From these calculations we conclude that regardless of the $H_2S$ line shape, there must be a larger microwave opacity in Neptune's atmosphere than in that of Uranus, which can be accomplished by assuming the $H_2S$ abundance to be larger on Neptune ($\gtrsim 5\times$) than on Uranus.

The effect of a change in the line shape on Neptune's spectrum is shown in Fig. 9. In these calculations $H_2S$ is enhanced by a factor of 20 above solar S, and $H_2O$ and $NH_3$ are equal to the solar O and N values, respectively. The width of the $H_2S$ line was taken to be equal to 0.3, 1, and $3\times$ that of $H_2O$. Note that if $H_2S$ is enhanced by a factor of 20 above solar, Neptune's spectrum can be matched best if the line width is $3\times$ broader than that of water, while Uranus' spectrum required a linewidth $3\times$ smaller than that of water. This is consistent with our conclusion above that the opacity in Neptune's atmosphere must be larger than that in Uranus' atmosphere.

If we increase the water mixing ratio to equal the enhancement in $H_2S$, the effect on the microwave spectrum is very small. Changes in the $NH_3$ mixing ratio from 0.1 to $10\times$ solar N affect the spectrum somewhat near the

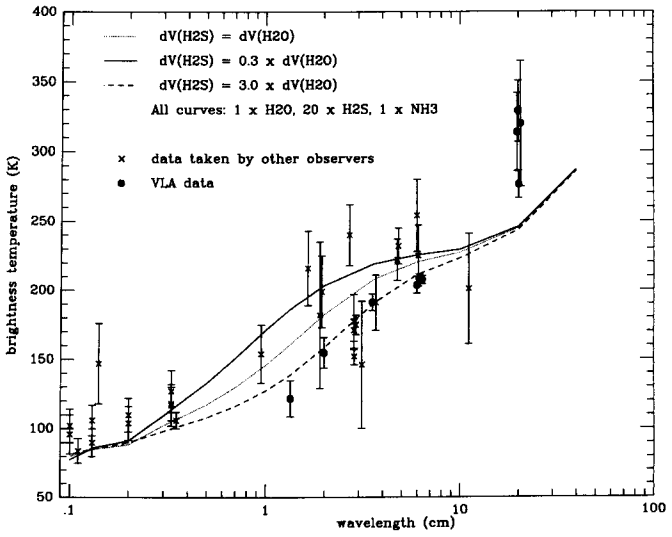


FIG. 9. Neptune's spectrum with calculations to show the effect of a change in the $H_2S$ line shape. The calculations are for an atmosphere with $20\times$ solar $H_2S$, and solar abundances for $H_2O$ and $NH_3$. The width of the line shape was taken to be 0.3, 1, and $3\times$ the width of the $H_2O$ line shape.

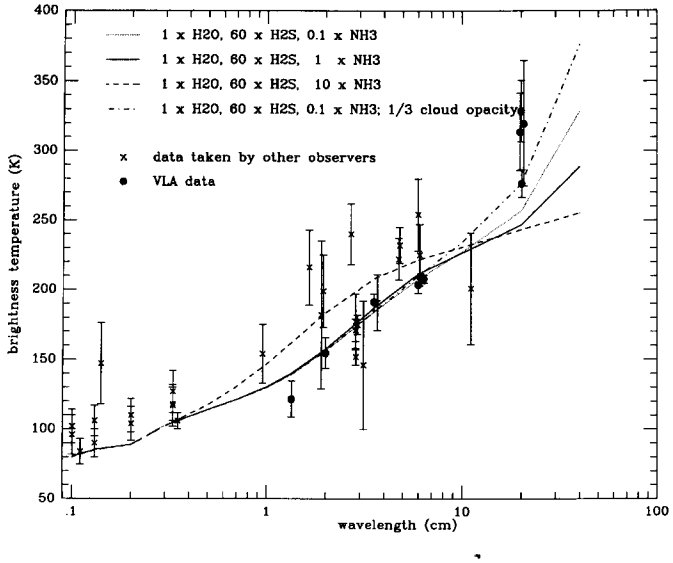


FIG. 10. Neptune's spectrum with superimposed model calculations for an atmosphere in which $H_2S$ is enhanced by a factor of 60 above solar S, and $NH_3$ by a factor of 0.1, 1, and 10 above solar N, respectively.

20-cm wavelength. Figure 10 shows results of calculations for a model atmosphere in which $H_2S$ is enhanced by a factor of 60 above solar S, $H_2O$ is kept solar, and $NH_3$ is taken as 0.1, 1, and 10× solar N. The dot–dashed curve shows the result for the first model if the cloud opacity is only one-third of the expected value. Like in the case of Uranus, both the ammonia abundance and cloud opacity have to be decreased to get a precise fit through the new 20-cm data point. Although a decrease in the cloud density is reasonable, it is unlikely that the N/H ratio is much below the solar value based upon current theories on the formation and evolution of the Solar System. Note further that the brightness temperature of the third model (10 × $NH_3$) lies above the other curves between 1 and 10 cm; this is due to the combined effect of a larger loss of $H_2S$ gas into the $NH_4SH$ layer, and the fact that this cloud layer is pushed to deeper levels in the atmosphere.

### *3d. Supersaturation?*

We compared our results regarding Uranus' and Neptune's microwave opacities with those obtained from the radio occultation experiments aboard Voyager (Lindal *et al.* 1987, 1990; Tyler *et al.* 1989). On Uranus, a depth of 2.3 bar, at a temperature of 101 K was reached during the occultation. At this temperature the mixing ratios for $NH_3$ and $H_2S$ follow the saturated vapor curves, and are $\sim 10^{-26}$ and $\sim 10^{-7}$, respectively, so the absorption at 3.6 cm is very small: $\sim 10^{-28}$ cm$^{-1}$ and 2–3 × $10^{-12}$ cm$^{-1}$ for $NH_3$ and $H_2S$, respectively. Hence they could and did not detect microwave absorption in the occultation data. On Neptune they probed down to a depth of 5–6 bar, at ~130 K level. They did detect microwave absorption, which was attributed to $NH_3$ gas. At this temperature, it is expected that both $NH_3$ and $H_2S$ gas will follow the saturated vapor curve. In absence of the formation of the $NH_4SH$ cloud, the mixing ratios of $NH_3$ and $H_2S$ are $\sim 7 \times 10^{-7}$ and $\sim 7 \times 10^{-5}$, respectively, resulting in an absorption of $\sim 3 \times 10^{-8}$ cm$^{-1}$ and $\sim 4 \times 10^{-9}$ cm$^{-1}$, respectively. If the $NH_4SH$ cloud is allowed to form, the mixing ratio of ammonia gas is much smaller, $\sim 10^{-19}$, which results in an absorption coefficient of $\sim 10^{-20}$ cm$^{-1}$.

Lindal *et al.* (1990) derived an ammonia mixing ratio of 600 parts per billion at 130 K, 6 bar to match the microwave opacity in their data. This number agrees with the saturated vapor values above ammonia–ice at this temperature and pressure. Since the absorption due to this concentration of ammonia gas is roughly an order of magnitude larger than that due to $H_2S$ gas (if the line width is similar to or less than that of water), they may indeed have detected opacity due to $NH_3$, rather than $H_2S$ gas in Neptune's atmosphere.

Since model atmosphere calculations in chemical equilibrium predict the formation of $NH_4SH$, the ammonia abundance is expected to follow the saturated vapor curve above the $NH_4SH$ cloud. The observations of Lindal *et al.* (1990) imply supersaturation of ammonia gas above the $NH_4SH$ cloud. The $NH_3$ abundance they derived at 130 K is $\sim 6 \times 10^{-7}$, which implies supersaturation of this gas in the atmosphere at levels where $T \lesssim 210$–225 K, or $P \lesssim 20$–25 bar for an $H_2S$ ratio enhanced by a factor of 10–100 above solar. Since much of the microwave opacity in this supersaturated atmosphere is due to ammonia gas, the $H_2S$ abundance does not need to be very high. Figure 11 shows calculations for a supersaturated atmosphere, with $NH_3 = 6 \times 10^{-7}$, in which $H_2S$ is enhanced by factors of 5, 10, 30, and 100, respectively.

Since the $NH_3$ mixing ratio derived by Lindal *et al.* (1990) referred to their deepest entry point, the abundance could be larger below that level. Obviously, when the ammonia mixing ratio is increased, the shape of the spectrum changes as well. An example is shown in Fig. 12, where $H_2S$ is kept equal to 10× solar, and $NH_3$ is supersaturated at $6 \times 10^{-7}$, $1 \times 10^{-6}$, and $3 \times 10^{-6}$, respectively. One can see that increasing $NH_3$ much above $1 \times 10^{-6}$ lowers the synthetic spectra too much. If the opacity due to $H_2S$ is negligible, as, e.g., for a solar abundance, the spectrum can be matched with $NH_3$ equal to $3.0 \times 10^{-6}$, as was shown in Fig. 7.

If Neptune's atmosphere is supersaturated, we may expect a similar phenomenon on Uranus. If $H_2S$ is enhanced 10× solar, and the line shape is equal to that of $H_2O$, one can constrain the $NH_3$ mixing ratio to $\lesssim 10^{-7}$ on Uranus; this number depends slightly (within a factor of a few) upon both the $H_2S$ mixing ratio and line profile. On Neptune, for a similar atmosphere, $NH_3$ gas is most likely

supersaturated at $\sim 10^{-6}$, an order of magnitude larger than in Uranus' atmosphere.

PRA suggested that supersaturation of $NH_3$ with respect to $NH_4SH$ on Uranus and Neptune may be plausible. The reaction $H_2S + NH_3 \rightarrow NH_4SH$ is heterogeneous and thus requires the presence of condensation nuclei. PRA suggested that, based upon calculations on the sedimentation, sublimation, condensation, and growth of the particles, the air on Uranus and Neptune above the 220–240 K level could have been cleared of condensation nuclei.

### *3e. Cloud Structure*

Figure 13 illustrates the locations and densities of the various clouds as a function of temperature and pressure on Uranus and Neptune. The $H_2O$–ice cloud in these figures is indicated by a dotted curve and the solution cloud by a dashed line to help the reader distinguish the various cloud layers. For these cloud models we assumed an atmosphere with solar abundances for $H_2O$ and $NH_3$, and an enhancement in $CH_4$ by a factor of 30 above solar C. $H_2S$ was taken to be enhanced above solar S by a factor of 10 on Uranus and 30 on Neptune. We assumed $NH_3$ gas to be supersaturated in Neptune's atmosphere at temperatures $T \lesssim 215$ K (pressures $P \lesssim 22$ bar), with a mixing ratio of $6.0 \times 10^{-7}$, as implied by the radio occulation experiment aboard Voyager (Lindal *et al.* 1990). The presence of this gas at these levels in the atmosphere will trigger the formation of a small ammonia ice cloud at the ~4-bar pressure level, as indicated on Fig. 13b. Based upon planetary formation theories, Pollack and Bodenheimer (1989) suggest the water mixing ratio to be enhanced by the same factor or more above solar O than that of $H_2S$ above solar S. If the water mixing ratio is enhanced to 10× solar O on Uranus, and 30× solar on Neptune, the solution cloud is expected to extend to deeper levels in the atmosphere. This cloud is indicated by the lower dashed lines on Fig. 13.

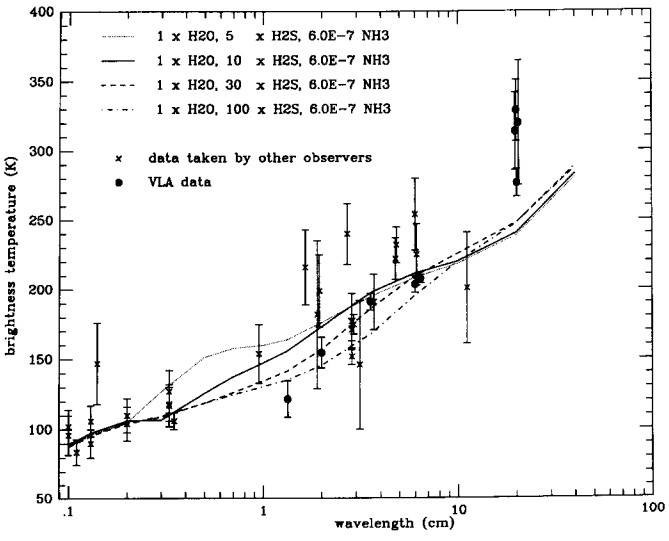


FIG. 11. Neptune's spectrum with superimposed calculations for an atmosphere in which ammonia gas is supersaturated at $6.0 \times 10^{-7}$, at levels where $T \lesssim 210$–225 K (see text), up to ~120–130 K, where the ammonia ice cloud starts to form. Curves for $H_2S$ mixing ratios of 5, 10, 30, and 100× solar are indicated. The $NH_3$ and $H_2O$ abundances deep in the atmosphere are solar.

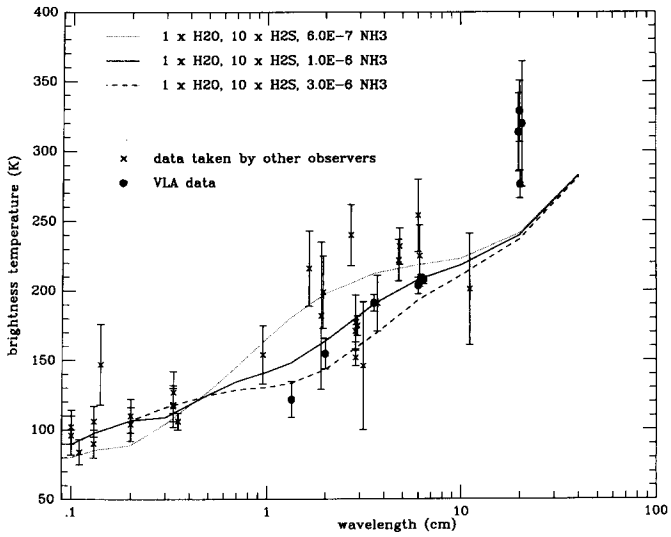


FIG. 12. Neptune's spectrum with superimposed calculations for an atmosphere in which ammonia gas is supersaturated at $6 \times 10^{-7}$, $1 \times 10^{-6}$, and $3 \times 10^{-6}$, respectively. The $H_2S$ mixing ratio was held constant at 10× solar. The $NH_3$ and $H_2O$ mixing ratios deep in the atmosphere are solar.

From ground-based spectroscopic observations it has been suggested for both Uranus (Baines and Bergstrahl 1986) and Neptune (Hammel *et al.* 1989) that there is a cloud layer below the methane–ice cloud with its cloud top at around the 3-bar level. Our model calculations suggest the presence of an $H_2S$–ice cloud at around this level. For equal enhancements of $CH_4$ and $H_2S$ above solar C and S, respectively, the mass column density of the $H_2S$ cloud is half that of the $CH_4$ cloud.

## CONCLUSIONS

We observed Neptune with the VLA at 3.55 and 20.1 cm, on April 15–19, 1990. The disk-averaged brightness temperatures are: 191.2 ± 6 K at 3.55 cm, and 276.4 ± 10 K at 20.1 cm. The data are consistent with thermal emission from Neptune's atmosphere.

We investigated the effect of possible microwave absorption by $H_2S$ on the spectra of Uranus and Neptune. Even though the rotational lines of this gas are at wave-

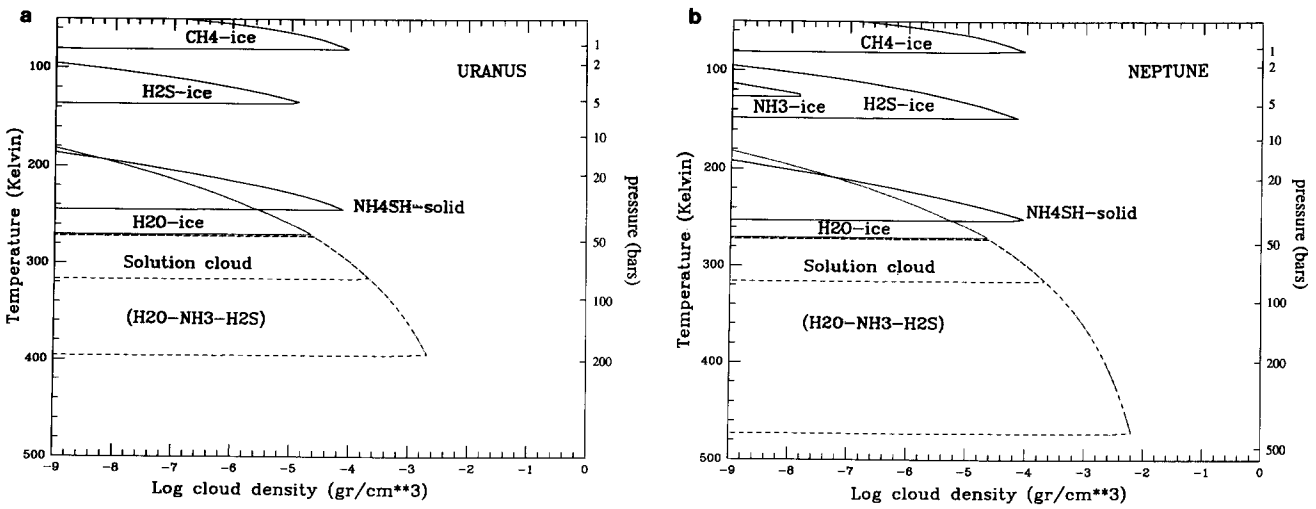


FIG. 13. The locations and densities (maximal values) of the various cloud layers in the atmospheres of Uranus and Neptune. The dotted line is for $H_2O$–ice and the dashed line for the solution cloud. The $CH_4$, $H_2S$, $NH_4SH$, and $NH_3$ (only on Neptune) clouds are shown by the solid lines. The bulk atmospheric composition for the calculations was for Uranus: 1 × $NH_3$, 10 × $H_2S$, and 1 × and 10 × $H_2O$ for the upper and lower dashed lines, respectively; for Neptune: 1 × $NH_3$, 30 × $H_2S$, and 1 × and 30 × $H_2O$ for the upper and lower dashed curves, respectively. The ammonia ice cloud only forms if there is rapid vertical mixing or supersaturation of the $NH_4SH$ cloud in the atmosphere; we assumed an ammonia mixing ratio of $6 \times 10^{-7}$ at $T < 215$ K for this calculation, the $NH_3$ mixing ratio as implied by the radio occultation experiment aboard Voyager (Lindal *et al.* 1990).

lengths less than a few millimeters, the lines are pressure broadened to such an extent that a large amount of opacity may be present at centimeter wavelengths. Using these new models, we estimate the $H_2S$ mixing ratio on Uranus and Neptune to be enhanced by a factor of 10–30 above solar S. These abundances may be consistent with models on the planet's interior structure and gravity field (Marley, Podolak, and Hubband 1990, private communication). In addition, the S/N ratio must exceed 5× solar. On Neptune, the total microwave opacity must be larger than that on Uranus to match the observed spectrum. The extra opacity is likely due to $NH_3$- rather than $H_2S$ gas (see below).

Unfortunately, the line width of $H_2S$ has never been measured under Uranian/Neptunian conditions. According to our calculations the width should be similar to or less than that of water.

We compared our results with those from the radio occultation data by Tyler *et al.* (1986) and Lindal *et al.* (1987, 1990). On Uranus, the occultation data do not probe deep enough in the atmosphere to influence the microwave opacity; on Neptune, the data probe down to ~130 K, and they measure microwave opacity consistent with an $NH_3$ mixing ratio of $6 \times 10^{-7}$, the value expected for ammonia gas above ammonia–ice. We show that Lindal *et al.* (1990) may indeed have observed opacity due to $NH_3$ gas, rather than that due to $H_2S$ gas. This would imply that $NH_3$ gas in Neptune's atmosphere is supersaturated at levels where $T \lesssim 210$–$225$ K ($P \lesssim 20$–$25$ bar). Due to the microwave opacity of this amount of $NH_3$ gas, the $H_2S$ mixing ratio on Neptune may be similar to that on Uranus.

The pole-to-equator temperature gradient on Uranus suggests a large depletion of gases in the polar region (factor 50–100) and at midlatitudes (factor of 10), and an enhancement by a factor of ~5 in the equatorial region. This suggests a general upwelling of gas in the equatorial region, and subsidence at midlatitudes and in the polar region. This general model is consistent with the models proposed by Flasar *et al.* (1987) and by Hofstadter *et al.* (1990). It suggests that at least part of Uranus' heat redistribution is controlled by the internal heat flux, despite the fact that this seems inconsistent with current radiative–convective–dynamic models of the Giant planet atmospheres.

We further note that no atmospheric model with both gas and cloud opacity sources perfectly fits the data, in particular the data at wavelengths longward of ~4–6 cm. There seems to be less opacity in Uranus and Neptune's atmosphere than indicated by our models. This is most likely due to an overestimate of the solution cloud density by the model and thus cloud opacity. As the model cloud densities are the maximum possible cloud densities this is not surprising. Good fits are obtained if both the ammonia mixing ratio is low and the cloud densities are reduced by a factor of 3. A reduction of the cloud densities is quite reasonable as a similar reduction from model predicted densities is required to match observations of terrestrial

clouds. A subsolar N/H ratio, if it persists throughout the atmosphere, is more of a concern based upon current theories on the formation and evolution of our Solar System.

The major source of error in the research described in this paper is the uncertainty in the line shape of $H_2S$ gas. We strongly encourage microwave spectroscopists to measure the line broadening of $H_2S$ at microwave wavelengths in an $H_2$–He–$CH_4$ gas mixture at high pressures ($\gtrsim$5–10 bar). Accurate knowledge of this shape will enable us to place firmer limits on the mixing ratios of $H_2S$ and, possibly, $NH_3$ gas, as well as the particle densities in the cloud layers.

## ACKNOWLEDGMENTS

We thank S. Gulkis, J. Joiner, W. J. Welch, B. Bezard, and G. O. Bjoraker for discussions regarding microwave absorption of $H_2S$, and M. Standish for providing an accurate ephemeris for Neptune. We also thank M. S. Marley, M. Podolak, and W. B. Hubbard for discussions regarding the interior structure of the planets and their gravity field, and M. Flasar for discussions regarding the dynamics in Uranus' atmosphere. IdP acknowledges support from NSF Grant AST-8900156. P.N.R. acknowledges support from NASA Contract NAS5-30134 at NASA–Goddard Space Flight Center, and S.K.A. acknowledges support received from NASA Grant NAGW-1771.

## REFERENCES

ANDERS, E., AND N. GREVESSE 1989. Abundances of the elements: meteoritic and solar, *Geochim. Cosmochim. Acta* **53,** 197–214.

BAARS, J. W. M., R. GENZEL, I. I. K. PAULINY-TOTH, AND A. WITZEL 1977. The absolute spectrum of Cas A: An accurate density scale and a set of secondary calibrators. *Astron. Astrophys.* **61,** 99–106.

BAINES, K. H., AND J. T. BERGSTRAHL 1986. The structure of the Uranian atmosphere: Constraints from the geometric albedo spectrum and $H_2$ and $CH_4$ line profiles. *Icarus* **65,** 406–441.

BERGE, G. L., AND S. GULKIS 1976. In *Jupiter* (T. Gehrels, Ed.), pp. 621–692, Univ. of Arizona Press, Tucson.

BEZARD, B., A. MARTEN, J. P. BALUTEAU, D. GAUTIER, J-M. FLAUD, C. C. PEYRET 1983. On the detectability of $H_2S$ in Jupiter. *Icarus* **55,** 259–271.

CAMERON, A. G. W. 1982. Elemental and nuclidic abundances in the solar system. In *Essays in Nuclear Astrophysics* (C. A. Barnes, D. D. Clayton, and D. N. Schramm, Eds.), pp. 23–43, Cambridge Univ. Press, London/New York.

CLARK, B. G. 1980. An efficient implementation of the algorithm "CLEAN." *Astron. Astrophys.* **89,** 377.

CONRATH, B., D. GAUTIER, R. HANEL, G. LINDAL, AND A. MARTEN 1987. The Helium abundance of Uranus from Voyager measurements. *J. Geophys. Res.* **92,** 15,003–15,010.

CONRATH, B. J., J. C. PEARL, J. F. APPLEBY, G. F. LINDAL, G. S. ORTON, AND B. BEZARD 1988. *Thermal structure and heat balance of Uranus, paper presented at Uranus Colloquium, Pasadena, June 28 to July 1, 1988.*

DE PATER, I. 1990. Radio images of planets, *Annu. Rev. Astron. Astrophys.* **28,** 347–399

DE PATER, I., AND C. K. GOERTZ 1989. Synchrotron radiation from Neptune: Neptune's magnetic field and electron population. *Geophys. Res. Lett.* **16,** 97–100.

DE PATER, I., AND S. GULKIS 1988. VLA Observations of Uranus at 1.3–20 cm. *Icarus* **75,** 306–323.

DE PATER, I., AND MASSIE, S. T. 1985.Models of the millimeter–centimeter spectra of the Giant planets, *Icarus* **62,** 143–171.

DE PATER, I., AND M. RICHMOND 1989. Neptune's microwave spectrum from 1 mm to 20 cm. *Icarus* **80,** 1–13.

DE PATER, I., P. N. ROMANI, AND S. K. ATREYA 1989. Uranus' deep atmosphere revealed. *Icarus* **82,** 288–313.

FLASAR, F. M., B. J. CONRATH, P. J. GIERASCH, AND J. A. PIRAGLIA 1987. Voyager infrared observations of Uranus' atmosphere: Thermal structure and dynamics. *J. Geophys. Res.* **92,** 15,011–15,018.

FLAUD, J. M., C. CAMY-PEYRET, AND J. W. C. JOHNS 1983. The far-infrared spectrum of hydrogen sulfide. The (000) rotational constants of $H_2^{32}S$, $H_2^{33}S$, and $H_2^{34}S$, *Can. J. Phys.* **61,** 1462–1473.

FRIEDSON, J., AND A. P. INGERSOLL 1987. Seasonal meridional energy balance and thermal structure of the atmosphere of Uranus: A radiative convective–dynamical model. *Icarus* **69,** 135–156.

GIAUQUE, W. F., AND R. W. BLUE 1936. Hydrogen Sulfide. The heat capacity and vapor pressure measurements of solid and liquid. The heat of vaporization. A comparison of thermodynamic and spectroscopic values of the entropy. *J. Am. Chem. Soc.* **58,** 831–837.

GULKIS, S., AND I. DE PATER 1984. In *Uranus and Neptune, NASA Conference Publ. 2330, Proceedings of a workshop held in Pasadena, CA, Feb. 6–8, 1984,* p. 225–262.

GULKIS, S., M. J. JANSSEN, AND E. T. OLSEN 1978. Evidence for the depletion of ammonia in the Uranus atmosphere. *Icarus* **34,** 10–19.

GULKIS, S., E. T. OLSEN, M. J. KLEIN, AND T. J. THOMPSON 1983. Uranus: Variability of the microwave spectrum. *Science* **221,** 453–455.

HAMMEL, H. B., K. H. BAINES, AND J. T. BERGSTRAHL 1989. Vertical aerosol structure of Neptune: Constraints from Center-to-limb profiles. *Icarus* **80,** 416–438.

HOFSTADTER, M. D., G. L. BERGE, AND D. O. MUHLEMAN 1990. Vertical motions in the Uranian atmosphere: An analysis of radio observations. *Icarus* **84,** 261–267.

HÖGBOM, J. A. 1974. Aperture synthesis with a non-regular distribution of interferometer baselines. *Astron. Astrophys. Suppl.* **15,** 417–426.

INGERSOLL, A. P., AND C. C. PORCO 1978. Solar heating and internal heat flow on Jupiter. *Icarus* **35,** 27–43.

KRAUS, G. F., J. E. ALLEN, JR., AND L. C. COOK 1989. Vapor pressure measurements of hydrogen sulfide. *B.A.A.S.* **21,** 948.

LELLOUCH, E., T. ENCRENAZ, F. COMBES, AND P. DROSSART 1984. The observability of HCN on Jupiter in the millimeter range. *Astron. Astrophys.* **135,** 365–370.

LELLOUCH, E., T. ENCRENAZ, AND F. COMBES 1984. The observability of HCN and $PH_3$ on Saturn in the millimeter range. *Astron. Astrophys.* **135,** 371–376.

LEWIS, J. S., AND R. G. PRINN 1980. Kinetic inhibition of CO and $N_2$ reduction in the solar nebula. *Astrophys. J.* **238,** 357–364.

LINDAL, G. F., J. R. LYONS, D. N. SWEETNAM, V. R. ESHELMAN, D. P. HINSON, AND G. TYLER 1987. The atmosphere of Uranus: Results of radio occultation measurements with Voyager 2. *J. Geophys. Res.* **92,** 14,987–15,002.

LINDAL, G. F., J. R. LYONS, D. N. SWEETNAM, V. R. ESHELMAN, D. P. HINSON, AND G. L. TYLER 1990. The atmosphere of Neptune: Results of radio occultation measurements with the Voyager 2 spacecraft, *J. Geophys. Lett.*, **17,** 1733–1736.

ORTON, G. S., D. K. AITKEN, C. SMITH, P. F. ROUCHE, J. CALDWELL,

R. SNYDER 1987. The spectra of Uranus and Neptune at 8–14 and 17–23 $\mu$m. *Icarus* **70,** 1–12.

PEARL, J. C., B. J. CONRATH, R. A. HANEL, J. A. PIRRAGLIA, AND A. COUSTENIS 1990. The albedo, effective temperature, and energy balance of Uranus, as determined from Voyager IRIS data. *Icarus* **84,** 12–28.

POLLACK, J. B., AND P. BODENHEIMER 1989. *Origin and Evolution of Planetary and Satellite Atmospheres* (S. K. Atreya, J. B. Pollack, and M. S. Matthews, Eds.), pp. 564–602. Univ. of Arizona Press, Tucson.

POYNTER, R. L., AND H. M. PICKETT 1981. *Submillimeter, Millimeter and Microwave Spectral Line Catalogue.* JPL Publication 80-23.

PRUPPACHER, H. R., AND J. D. KLETT 1980. *Microphysics of Clouds and Precipitation.* Reidel, Dordrecht.

ROMANI, P. N., I. DE PATER, AND S. K. ATREYA 1989. Neptune's deep atmosphere revealed. *Geophys. Res. Lett.* **16,** 933–936.

SRAMEK, R. A., AND F. R. SCHWAB 1989. In *Synthesis Imaging in Radio Astronomy.* (R. A. Perley, F. R. Schwab, and A. H. Bridle, Eds.), pp. 117–138 NRAO Workshop No. 21, Astronomical Society of the Pacific.

STONE, E. C., A. C. CUMMINGS, M. D. LOOPER, R. S. SELESNICK, N. LAI, F. B. MCDONALD, J. H. TRAINOR, D. L. CHENETTE 1989. Energetic charged particles in the magnetosphere of Neptune. *Science* **246,** 1489–1494.

TYLER, G. L., D. N. SWEETNAM, J. D. ANDERSON, J. K. CAMPBELL, V. R. ESHELMAN, D. P. HINSON, G. S. LEVY, G. F. LINDAL, E. A. MAROUF, R. A. SIMPSON 1986. Voyager 2 Radio Science observations of the Uranian system: Atmosphere, rings, and satellites. *Science* **233,** 79–84.

TYLER, G. L., D. N. SWEETNAM, J. D. ANDERSON, S. E. BORUTSKY, J. K. CAMPBELL, V. R. ESHELMAN, D. L. GRESH, E. M. GURROLA, D. P. HINSON, N. KAWASHIMA, E. R. KURSINSKI, G. S. LEVY, G. F. LINDAL, J. R. LYONS, E. A. MAROUF, P. A. ROSEN, R. A. SIMPSON, AND G. E. WOOD 1989. Voyager Radio Science observations of Neptune and Triton. *Science* **246,** 1466–1473.